Chapter-1

Introduction and Literature Review

CHAPTER 1: Introduction and Literature Review

1.1 Introduction

Energy is considered as central to almost all major challenges that the world is facing today. As the world's economy and the population continuously grow, the corresponding energy requirement increases [1]. Fig. 1.1 represents the history and projection of world energy consumption by various energy sources up to the year 2050 and the global energy consumption by fuel type[1]. There are many sources of energy, such as traditional sources of energy, fossil fuels, nuclear sources of energy etc. Currently, fossil fuels are used as a major energy resource; however, the availability of fossil fuels is finite. When burned, fossil fuels give off carbon dioxide, which is the primary cause of the greenhouse effect leading to global warming. Over the last few decades, fossil fuel emissions have increased the concentration of carbon dioxide in the atmosphere above 400 ppm and caused a temperature increase of the world approx by 1 ℃. Mining this fossil fuel is also difficult and may endanger peoples' lives. Prolonged use of carbon-emitting fuel sources will exacerbate this trend resulting in devasting climate change. Nuclear power is a relatively clean energy source, but highly radioactive waste is the major concern. The limited fossil fuel reserves and continual ecological degradation have forced governments and industries to seek out renewable energy sources and power production technologies.

As a result, due to ever-increasing energy demands in the future, there is no choice but to prepare for the new era of renewable energy production such as wind, solar and hydro-power

systems. These alternative energy sources are rapidly growing and gaining popularity worldwide. However, because these renewable energy sources are generally dependent on the weather and are less efficient, their extensive expansion is limited. Wind turbines need wind to turn on their blades, and solar collectors need sunlight to gather heat and generate power. In addition, the current price of renewable energy is significantly higher than that of traditional fossil fuels. Furthermore, they are less efficient and non-portable. To address these constraints, ongoing attempts are being made to produce superior, highly efficient, and long-term energy conversion systems. Fuel cells are one of the promising technologies that is expected to meet most of these requirements. This "green" technology is gaining popularity with facilities looking to implement an environment-friendly electric power generation system without sacrificing efficiency, performance and availability.

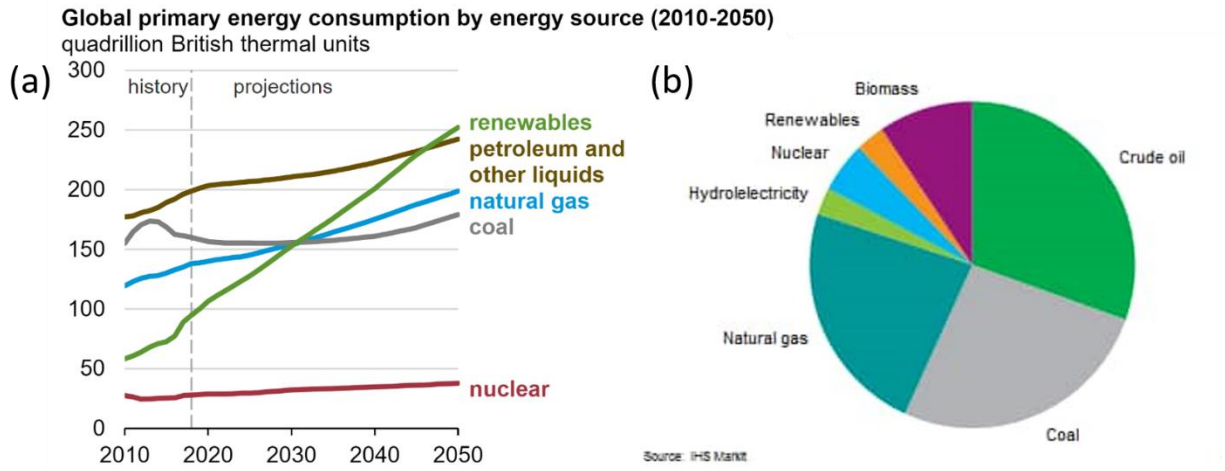

Figure 1.1: (a) World energy consumption by different energy sources with projection from 2010 to 2050. (b) Energy consumption by fuel type[1].

1.2 Fuel Cells: An Overview

A fuel cell is an electrochemical device that converts the chemical energy of reactants (fuel and oxidants) into electrical energy by utilising the natural tendency of oxygen and hydrogen to react. The efficiency of the fuel cell is generally high, owing to the direct conversion of chemical energy into electrical energy. The additional advantage that fuel cells offer over traditional Carnot-based energy systems is that they produce fewer emissions. The fuel cell has much fewer moving parts than the combustion engine, leading to a reliable and long-lasting system. They are ideal for a wide range of applications starting from mobile power systems to stationary power plants up to 1MW of power production. It is a simple device containing four main components: anode, cathode, electrolyte and interconnects.

The fuel cell was first identified by Sir William Robert Grove in the nineteenth century as the reverse process of electrolysis of water. In 1842, Groove sketched the design of fuel cells, and it is similar to today's phosphoric acid fuel cell. The diagram of the first fuel cell is depicted in Fig. 1.2. The system used platinum as the electrode and sulphuric acid as the electrolyte material. The electrochemical reaction on the electrode of fuel cell are:

$$\text{Anode: } H_2 \rightarrow 2H^+ + 2e^-$$

$$\text{Cathode: } {}^1\!/_2\, O_2 + 2e^- + 2H^+ \rightarrow H_2O \qquad (1.1)$$

$$\text{Overall: } H_2 + {}^1\!/_2\, O_2 \rightarrow H_2O$$

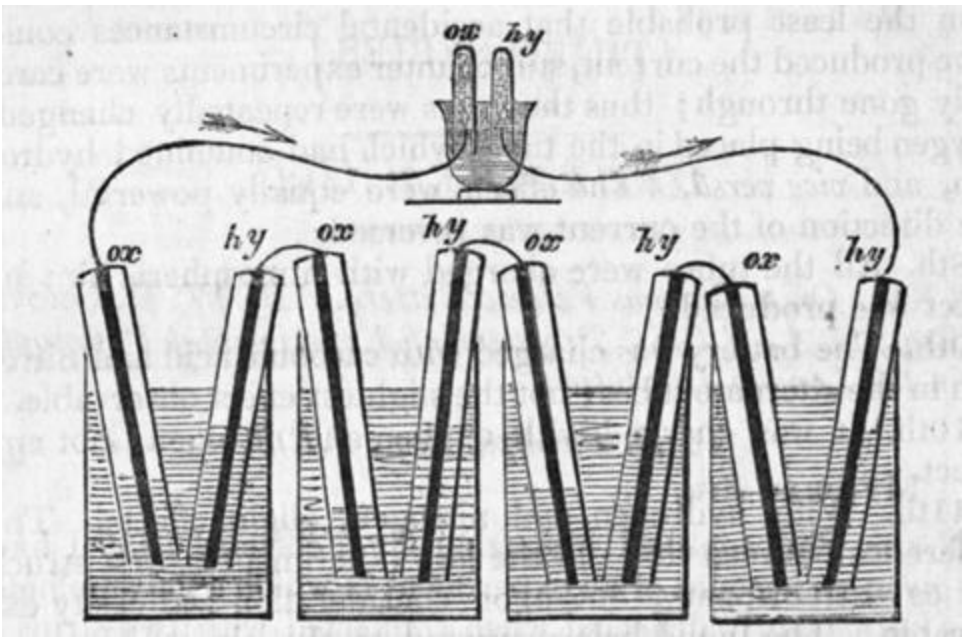

Figure 1.2: William Groves battery diagram[2]

1.2.1 Fuel Cell Efficiency

The efficiency of a traditional heat engine with maximum temperature T_1 and heat sink temperature T_2 is calculated as follows:

$$\text{Carnot Limit} = \frac{T_1 - T_2}{T_1} \qquad (1.2)$$

This limit is because of the unavoidable waste of heat energy proportional to T_2. Usually, the efficiency increases with the operating temperature of the heat engine (Fig. 1.3).

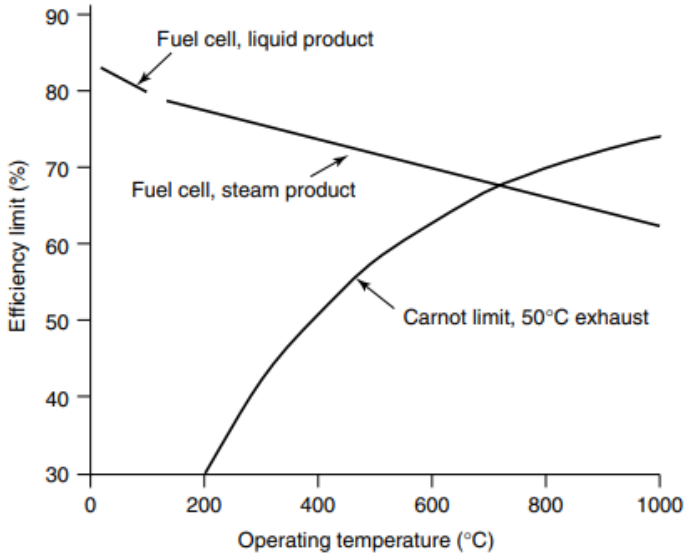

Figure 1.3: Maximum efficiency of hydrogen fuel cell with the steam produced compared to Carnot limit with 50 ºC exhaust temperature[3]

The efficiency of the fuel cell is generally expressed as the ratio of electrical energy converted per mole, $\Delta\bar{G}_f$, and enthalpy released per mole, $\Delta\bar{H}_f$, by the equation: $\eta = \frac{\Delta\bar{G}_f}{\Delta\bar{H}_f}$. Dissimilar to heat engine, the efficiency of fuel cell having H_2 as fuel decreases with temperature as Gibbs free energy, $\Delta\bar{G}_f$ become less negative with temperature due to greater contribution of entropy at the higher temperatures. Different fuel cell have different Gibbs free energy with temperature, and thus fuel cell with different fuels shows different maximum efficiencies at operating temperature.

Apart from the fuel contribution, activity of reactants (a_{H_2}, a_{O_2}) and products (a_{H_2O}) at triple-phase boundary also add to Gibbs free energy, and this can be anticipated by using the Nernst equation,

$$\Delta\bar{G}_f = \Delta\overline{G_f^0} + RT.ln\left(\frac{a_{H_2O}}{a_{H_2}.{a_{O_2}}^{1/2}}\right) \qquad (1.3)$$

where, T is temperature in Kelvin and R is gas constant. It is assumed that at high operating temperature gases behaves ideally, and thus the activity of gases is identical to the partial pressure, $a_{H_2} \approx \frac{p_{H_2}}{p^0}$. So the efficiency can be written as:

$$\Delta \bar{G}_f = \Delta \overline{G_f^0} + RT.ln\left(\frac{p_{H_2O}}{p_{H_2}.{p_{O_2}}^{1/2}}\right) \quad (1.4)$$

The partial pressure of gases associated with the reactions are factors that regulate the efficiency of the fuel cell system.

1.2.2 Fuel cell voltage

Electrical energy is the product of charge and electrical potential. Equation 1.1 associates two electrons, thus

Electrical energy converted = -2FE

where F represents Faraday constant, and E is electric potential. If the system is reversible, electrical energy = $\Delta \bar{G}_f$ = -2FE, thus

$$E = -\frac{\Delta \bar{G}_f}{2F} \quad (1.5)$$

This is known as the open circuit voltage (OCV) for the fuel cell operation.

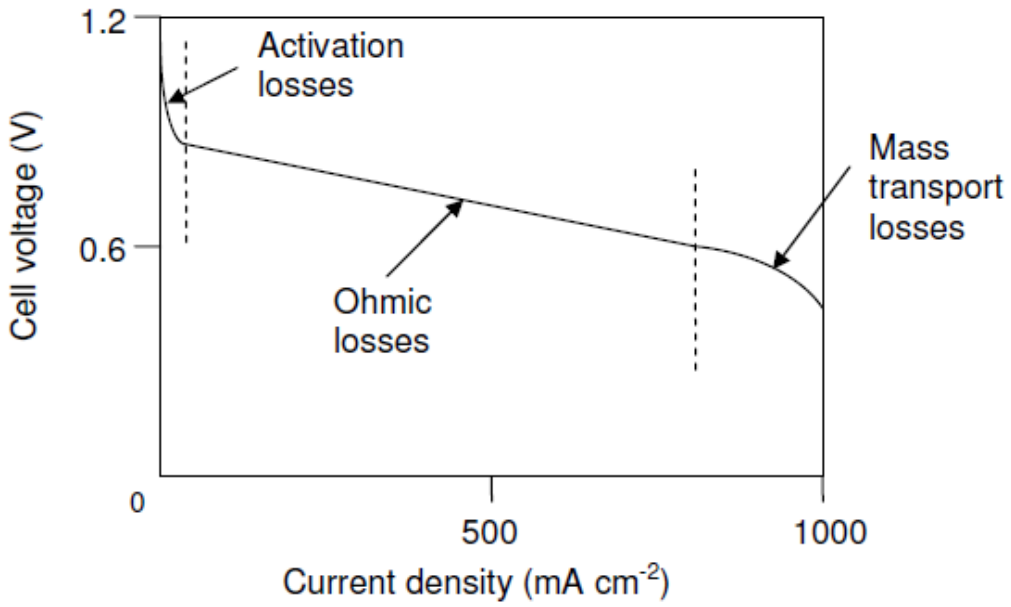

Figure 1.4: Plot indicating for a low temperature fuel cell fed with air and hydrogen[4]

In practice, a lower value of output voltage is achieved due to various losses involved in fuel cell operation,

$$V_{cell} = E_{thermo} - V_{act} - V_{ohmic} - V_{conc} \quad (1.6)$$

where V_{cell} is the output voltage under load, E_{thermo} is the thermodynamically predicted reaction potential, V_{act} is the activation polarization loss caused by limited reaction rate at the surface of cathodes, V_{ohmic} is the ohmic loss caused by resistance offered by the electrolyte to flow of ions and electrons by the electrolyte and electrode, and V_{conc} is the mass transport loss associated with the loss of concentration of fuel or oxidants at the surface of anode.

1.3 Fuel Cell Types

Fuel cells are categorized on the basis of the electrolyte material used. A list of the most promising type of fuel cells with their characteristics and reactions are depicted in table 1.1

and Fig. 1.5. Each system has its own advantage and disadvantage. Thus, distinct types of fuel cells are used for different types of applications.

For example, the Proton exchange membrane fuel cell (PEMFC) is optimal for mobile applications owing to its low operating temperature and use of solid membrane electrolytes. It uses solid polymer electrolyte, porous carbon electrodes with a platinum catalyst. The US government has been investigating PEMFC deliberately for the substitution of ICE in the transport sector[4]. However, the higher cost of sulfonated tetrafluoroethylene-based membrane, expensive catalyst, low resistance against carbon monoxide are the main problem in its commercialization.

The Alkaline fuel cell (AFC) can be produced at a lesser cost than that of the PEMFC because of its faster kinetics for oxygen reduction, owing to the high pH of the electrolyte. It utilized a range of non-precious metals as a catalyst. Furthermore, it uses a solution of potassium hydroxide as an electrolyte, which is much cheaper compared to the polymer proton exchange membrane, and thus an economic system. However, a key challenge for this type of system is its susceptibility to carbon dioxide (CO_2) poisoning. Even a small amount of CO_2 can dramatically alter the cell conductivity and its durability due to carbonate formation.

The solid oxide fuel cell (SOFC) is free from expensive metal catalysts owing to its high operating temperature and can operate with natural gas, methane, biogas and gases made from coal. It uses hard, dense ceramic as the electrolyte material with an efficiency of around 60%. Its efficiency is further improved by ingestion with classical thermodynamic technologies to utilize systems waste heat. SOFCs are sulphur resistant type fuel cells, and they are also not poisoned by carbon monoxide. However, its components compatibility and thermal shielding at high operating temperatures are challenging.

Table 1.1: Different types of fuel cells with their characteristics[5]

FuelCell Systems	**Electrolyte**	**Operating Temperature (℃)**	**Fuel**	**Application**	**Efficiency**
Proton exchange membrane (PEMFC)	Sulfonated PTFE membrane	30−100	H_2, methanol (DMFC)	Transportation Portable power	50-55%
Alkaline (AFC)	Potassium hydroxide	50−100	H_2	Speciality vehicles	50-55%
Phosphoric acid (PAFC)	Phosphoric acid	~200	H_2, CO	Large scale CHP	40-50%
Molten carbonate (MCFC)	Alkali metal carbonate	~650	H_2, CH_4, natural gas	Medium to large scale CHP	45-50%
Solid oxide (SOFC)	Ceramic	~500−1000	H_2, CH_4, natural gas	Small to large scale CHP	45-60%

The Phosphoric acid fuel cell (PAFC) utilizes H_3PO_4 as an electrolyte material and has been used for a long time for stationary power generation applications and commercial purposes. It is mainly used where uninterrupted power generation is required. It also utilizes combined heat and power to increase its efficiency. However, the requirement of an expensive platinum catalyst raises its cost.

Molten carbonate fuel cells (MCFC) are fuel cells that use a molten mixture of alkali metal carbonates retained in a porous lithium aluminium oxide matrix. As they operate at a high temperature of 650 ℃, non-precious metals can also act as catalysts, reducing costs. As opposed to other types of fuel cells, MCFCs use CO_2 and an oxidant to provide carbonate for ion exchange in the electrolyte. No reformer is required to convert fuel cells into hydrogen. Their main drawback is durability.

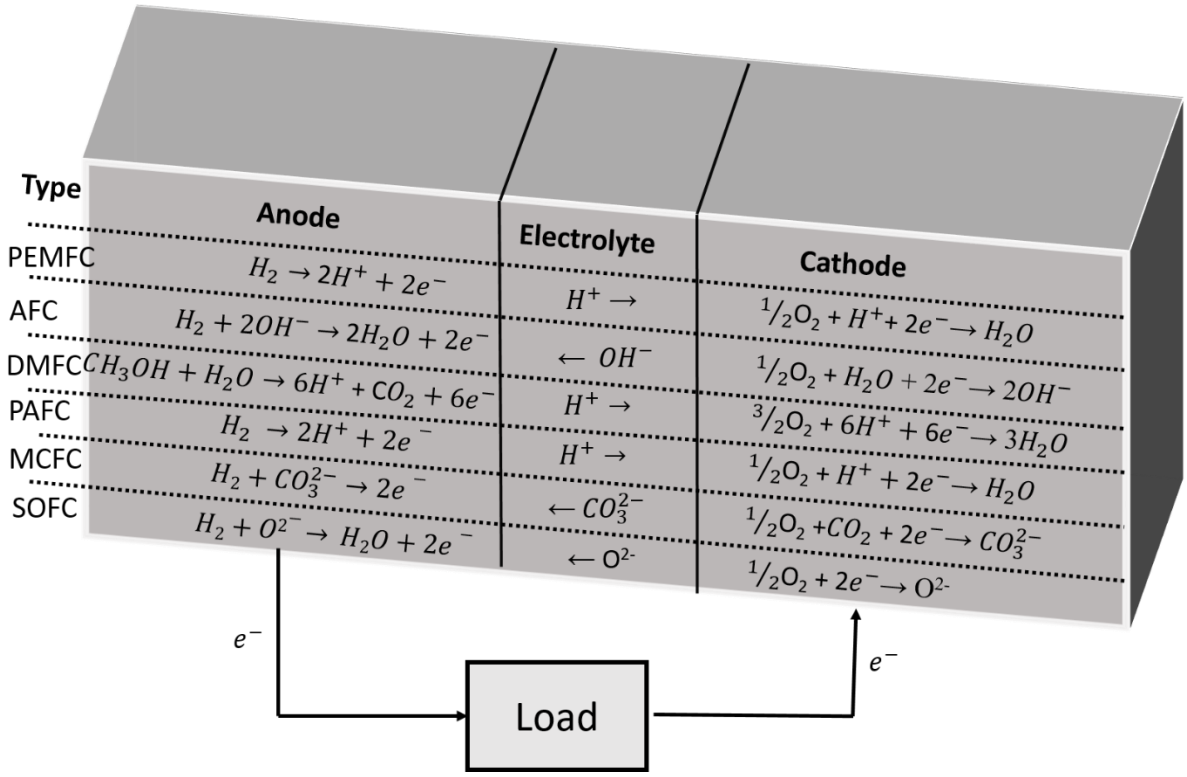

Figure.1.5: Reactions at electrodes for different types of fuel cells

1.4 Solid oxide fuel cell (SOFC)

Solid oxide fuel cell (SOFC) is a promising technology in terms of the overall efficiency it offers and its ability to operate with a variety of fuels. SOFC converts chemical energy directly into electrical energy, without the limitations of the Carnot cycle through the oxidation of fuels. The electrical power accessible from SOFCs ranges from a few Watts to several thousand watts[6]. SOFCs are emerging as new technologies to meet the current demand of energy, and it has the potential to revolutionize the current power supply system. The SOFC consists of layers of a dense electrolyte sandwiched between porous, permeable electrodes[7]. Depending on the electrolyte, SOFCs can either proceed via oxide ion or proton conduction. Electrical power generated from SOFC has the following general features:

- High power generation and thermal efficiency
- Easy to handle and durable
- Combined heat and power generation for industrial and domestic applications
- Operates on a wide range variety of hydrocarbon fuels and do not require expensive catalysts
- SOFCs are made up of ceramic material, which eliminates the problem of corrosion and liquid management problem of PAFC and MCFC
- Long term performance and durability

Furthermore, pollution level gets reduced by 20 – 40% with the reduction in CO_2 level per kW of electricity produced. SOFCs are classified into three categories based on their operating temperature: (i) Low-temperature SOFC (LT-SOFC): works in the 400-600 ℃ temperature range (ii) Intermediate temperature SOFC (IT-SOFC): works in the 400-600 ℃ temperature range (iii) High-temperature SOFC (HT-SOFC): works in the temperature range of 800-1000 ℃.

Since the present work focuses on the development of electrolyte materials for IT-SOFC applications, a brief discussion about the components and working principles of SOFC is being presented here.

1.5 Operation Principle

A typical SOFC schematic consisting of solid electrolyte placed between two electrodes are depicted in Fig. 1.6. At the cathode end, normally, air is supplied; therefore, it is called an air electrode.

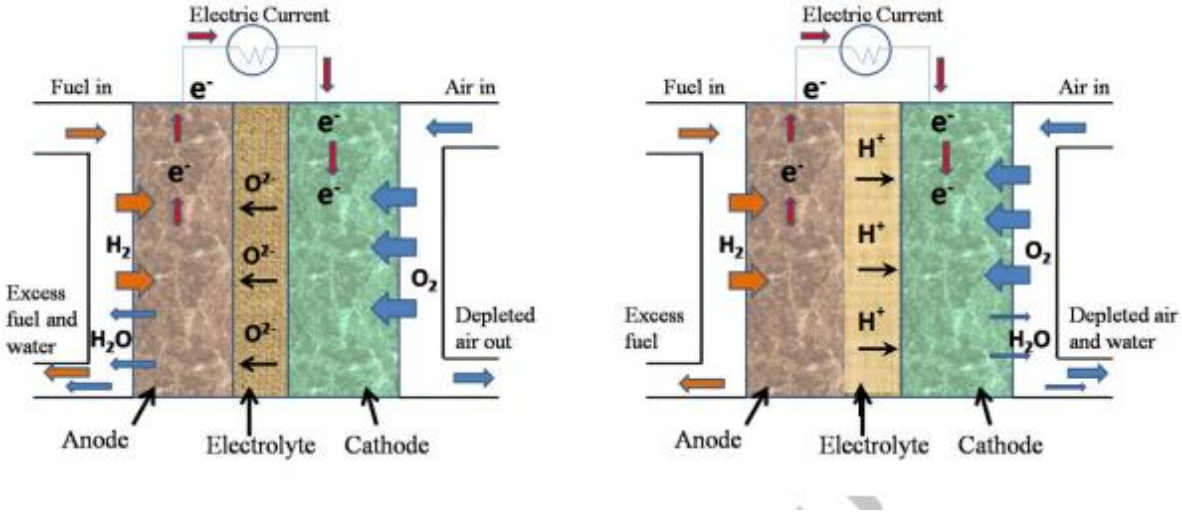

Figure 1.6: Schematic of working principle of (a) oxide ion conducting (b) proton-conducting SOFC[8]

There are two types of SOFC electrolytes: oxide ion and proton conductors. Though the conduction mechanisms of both types are quite different, operation principles are same for the both. During operation, oxygen from air travels from porous cathode to gas-cathode-electrolyte triple-phase boundaries, where it combines with the incoming electrons from the external circuit to form an oxide ion. The electrolyte conducts oxide ions to the electrolyte-anode interface, where they get electrochemically oxidized to liberate electrons and water. The electrons generated then pass through the external circuit containing a motor or electric load that consumes the power generated by the cell as per the chemical reactions shown in equations 1.1.

Proton conducting SOFC differs from the traditional SOFC in that the electrolyte membrane transports protons instead of oxygen ions. At the anode side of the cell, hydrogen is oxidized to protons and conducted through the electrolyte until it combines with oxygen at the cathode side to produce water. The electrons generated from the partial reaction are routed through the external circuit and thus produce electricity.

1.6 Components of SOFC

1.6.1 Oxygen electrode (Cathode)

A cathode or air electrode functions as the site for the electrochemical reduction of oxygen. It must have a porous structure to increase the specific surface area and allow the oxidants to reach the cathode-electrolyte interface. For an efficient operation, the cathode must possess the following properties:

- High electronic conductivity (preferably > 100 S/cm)
- High catalytic activity throughout oxidation-reduction reaction (ORR)
- Good chemical compatibility with the other cell components
- Cost-effective
- Minimal or comparable value of thermal expansion coefficient
- Resistance to thermal cycling

It is both an electric and ionic conductor. Meanwhile, it should have the ability of oxygen adsorption and catalytic cracking. The most common feature of the cathode materials are that the material should form oxygen adsorption bonds easily. The important reaction in the cathode is the oxygen adsorption process.

Prominent cathode materials: Doped lanthanum cobaltite & manganite (LSC & LSM), Lanthanum-Barium cobaltite (LBC), LSM-YSZ composite, $Pr_{0.06}Sr_{0.4}MnO_{3+\delta}$ (PSM), $Pr_{0.5}Sr_{0.5}FeO_{3-\delta}$ (PSF) etc.

1.6.2 Fuel electrode (Anode)

Anode is the place for electrochemical oxidation of the fuel, preferably at surface sites called triple-phase boundary. The oxidation reaction between the oxygen ions and hydrogen generates heat along with water and electricity. If the fuel is in the form of lighter hydrocarbon, (e.g. methane), then anode acts as the catalyst for steam reforming the fuel into hydrogen. It is both electronic and ionic conductor. Anode materials should meet the following requirements:

- Good catalytic activity towards hydrogen (or other fuel) oxidation reaction
- It should be porous for the passage of inlet fuels
- Thermal expansion coefficient of cathode material should match with the other cell components
- Chemical compatible with other components of the cell
- Chemically, mechanically, and thermally stable in the operating condition

Prominent anode materials: Ni-stabilized zirconia, Ni-Gadolinium doped ceria (Ni-GDC), La-doped Strontium titanate (LST), $Ba_{0.5}La_{0.5}In_{0.3}Ti_{0.1}Mn_{0.6}O_3$, $La_{0.65}Ce_{0.1}Sr_{0.25}Cr_{0.5}Mn_{0.5}O_{3-\delta}$ (LSCM).

1.6.3 Interconnect

An interconnect serves as the electric contact to the cathode and protects it from the reducing atmosphere of the fuel on the anode side. The high operating temperature of the cells combined with the harsh environment compels that interconnect must meet the most stringent requirement of the cell components. For proper functionalities of SOFC interconnect must possess the following properties:

- 100% electronic conductivity.
- Dense and free from porosity.
- Thermal expansion coefficient compatibility with the other component of fuel cell
- Cost-efficient.
- Stability in both oxidizing as well as reducing atmosphere since it is exposed to fuel on anode side and air on the cathode side
- Minimal P_{O_2} gradient in order to regulate dimensional change and and diminish mechanical stress

In general, there are two types of interconnect materials, i.e. metallic alloys and ceramics. Ceramic interconnects are evolved from semiconductor oxide. The conductivity of these oxides increases with the temperature, making them suitable for the high-temperature applications. However, at temperature below 600 ºC, conductivity is not significant. Most widely used ceramic interconnect are lanthanum chromite ($LaCrO_3$).

However, ease of fabrication and low cost have made metals more interesting than ceramic oxide as interconnect materials. With the metallic interconnects, it has been possible to reduce the operating temperature below 800 ºC.

Prominent interconnect materials: Cr-based alloys, $LaCrO_3$, $La_{0.95}Ca_{0.05}CrO_3$, Fe-Cr based alloys, Ni-Cr (Fe) based heat resistance alloys, ferric stainless steels, Austenitic stainless steel etc.

1.6.4 Electrolyte

The main component of the SOFC is the solid electrolyte. It is the heart of SOFC and transports the oxide ions without significant loss from cathode to anode. The transport of oxide

ions occurs through the oxygen vacancies in the oxygen sublattices. For attaining high ionic conductivity in electrolyte materials, crystal structure should possess low migration enthalpy and ample interionic open space[9]. The ionic conduction in a material is dependent on the ion diffusion efficiency of the substance[10][11]. Figure 1.7 depicts the representative diffusion mechanism for ion transport.

Vacancy diffusion. This type of diffusion is based on the vacancies in the crystal defects, and it takes place among the lattice site. Atom needs energy to break the bonds with the neighbours, jump from one lattice site to other and cause lattice distortion during the jump. This energy appears from the thermal energy of atomic vibrations and applied electric fields.

Interstitial diffusion. It is usually faster than vacancy diffusion as the bonding of interstitials to the surrounding atom is normally weaker, and there are more interstitial sites than vacancies to jump. It requires small amount of impurity atoms to fit into interstices into the host.

Ion exchange. In this, an ion is exchanged with other neighbour ions in the crystal. This mechanism creates local distortions within the crystal. However, this does not assume the existence of permanent point defects in the crystal.

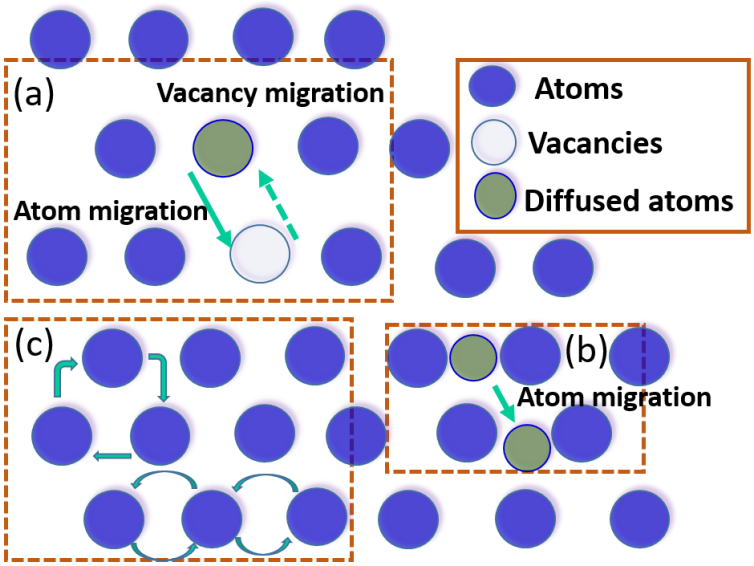

Figure 1.7: Schematic of ion diffusion mechanism (a) vacancy diffusion (b) Interstitial diffusion (c) ions exchange in solid state structure

The primary requirements of electrolytes to work efficiently are:

- Electrolyte should be thermally, chemically and structurally stable over a wide temperature range (RT-1000 ºC) and oxygen partial pressures (1 - 10^{-22} atm.)
- It should be chemically inert towards the electrodes both during processing and operation
- It must possess high ionic conductivity and no electronic conductivity
- It should be fully dense in order to prevent short-circuiting of reacting gases
- It should have comparable thermal expansion coefficient with the adjoining cell components
- It should be thin in order to minimize the cell's resistive losses

Prominent electrolyte materials: Scandia stabilized zirconia (ScSZ), Sr & Mg-doped Lanthanum gallate (LSGM), Hexagonal perovskites ($Ba_7Nb_{3.9}Mo_{1.1}O_{20.05}$) Yttria stabilized zirconia (YSZ), Brownmillerites ($Ba_2In_2O_5$), Bi_2O_3 based oxides, Sm/Gd doped ceria

(SDC/GDC), Lanthanum silicate apatite ($La_{10}Si_6O_{26}$), etc. Figure 1.8 compares the oxide ion conductivity of some prominent electrolyte materials.

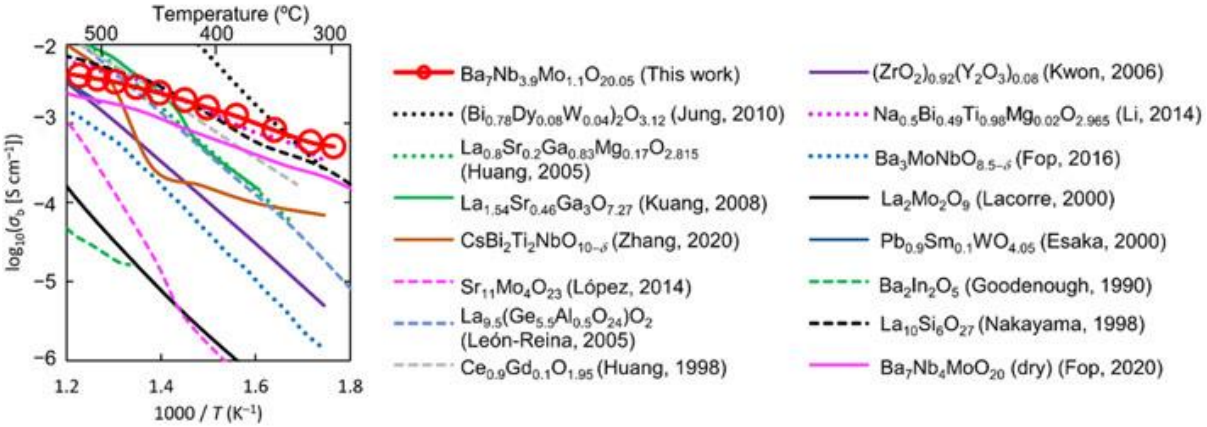

Figure 1.8: Comparative of bulk conductivity of prominent oxide ion conductors[12]

1.7 Factors influencing the ionic conductivity of an electrolyte

In electrolyte material, maximization of ionic conductivity is important. Many parameters can influence the ionic conductivity of electrolytes. Numerous efforts have been made to improve the ionic conductivity of the electrolyte. Composition, processing and microstructure are the parameters that affect the conductivity[13][10]. The schematic diagram shown in Fig. 1.9 illustrates the important factors responsible for ionic conduction in most of the oxide electrolytes.

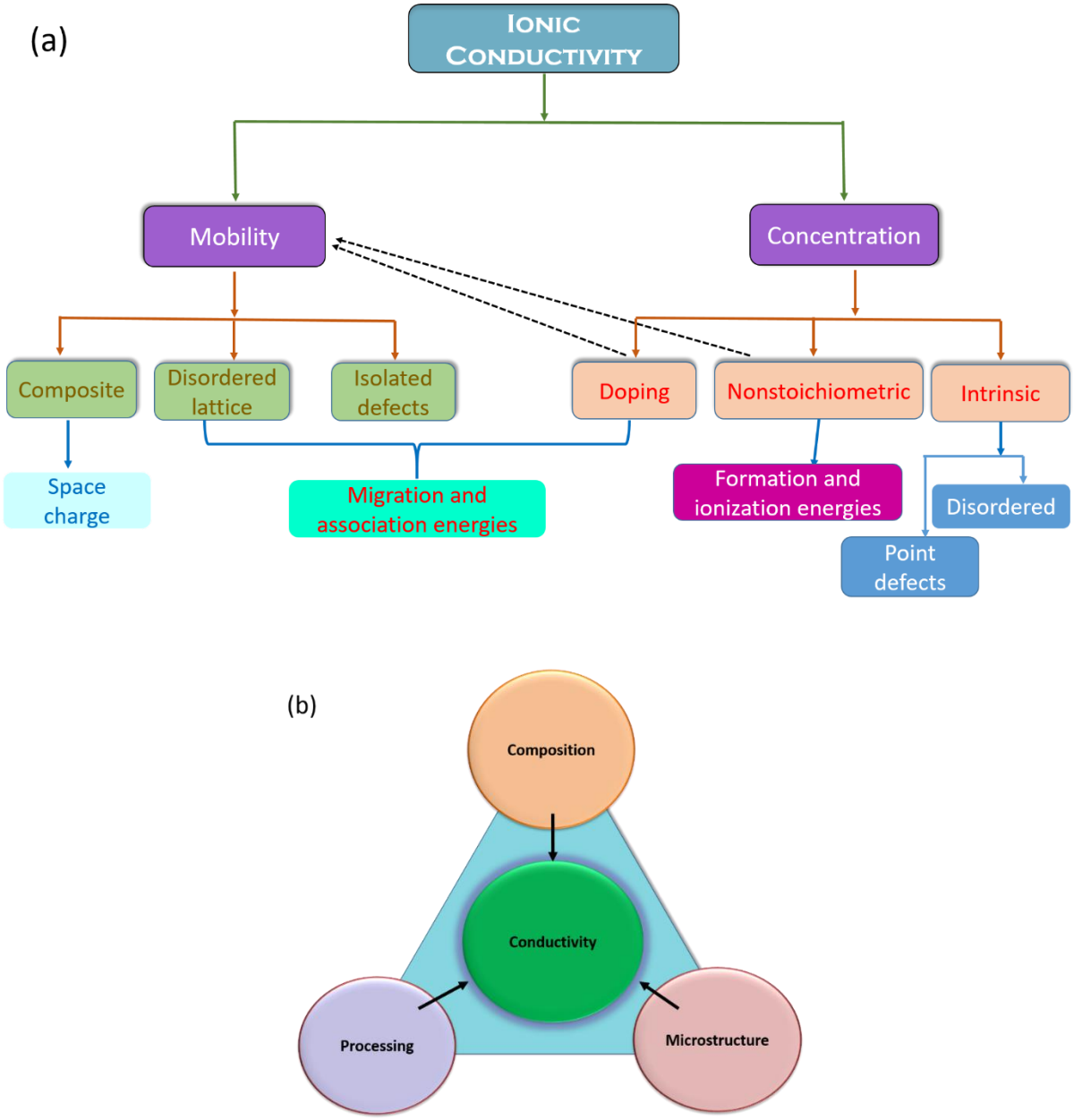

Figure 1.9: (a) Sources of ionic carriers in oxides **(b)** A correlation between material composition, processing, microstructure, and electrical conductivity

1.7.1 Conduction Process

Electrolyte materials must be investigated to control the specific variables that can optimize the level of ionic conductivity in a potential SOFC. Defects present in the crystal lattices are the key factor of ionic conduction. Many years have been spent studying the

mechanics of diffusion and ionic conductivity in order to better understand the variables involved in defect development and ionic mobility. Kofstad[14] proved that faults formed in crystal lattices at all temperatures above absolute zero using thermodynamic equations. Additionally, vacancies can be generated intrinsically within the crystal structure due to charge compensation when aliovalent cation dopants are substituted on the normal lattice site or as a function of temperature. The concentration of anion vacancies can be manipulated by the degree of cation aliovalent doping. This form of vacancy generation is the basis for ionic conductivity in SOFC electrolytes.

Since ionic motion occurs as ions hop through a lattice via defects when subjected to an electric field. Ion conduction rate is described by a very common equation (1.7) [15][16].

$$\sigma = nq\mu \qquad (1.7)$$

σ is ionic conductivity ($S.cm^{-1}$), q is the magnitude of charge for the oxygen ion (coulombs), n is the number of mobile ions in a given lattice volume (cm^{-3}), and μ is the mobility of the ions ($cm^2sec^{-1}V^{-1}$). The Einstein relationship [16][17] relates the mobility of ions across a lattice to the ionic self-diffusion coefficient. The ionic self-diffusion coefficient can be expanded further to consider three-dimensional, random walk motion through the lattice. Thus the resulting expression for the ionic mobility can be obtained as below[16][17].

$$\mu=[z/6][q/(kT)][1-c]\gamma\lambda^2\upsilon\exp[-\Delta G_m/(kT)] \qquad (1.8)$$

where z is given by the number of equivalent near (dimensionless), λ is the jump distance (cm), γ is a correlation factor (dimensionless units), υ is the attempt jump frequency (sec^{-1}), and ΔG_m is the free energy for ion motion (eV). According to Kilner[16], the correlation factor measures the atomic jumps' deviation from randomness, and in a basic cubic lattice, it would be 0.65. The word c is the fraction of equivalent sites occupied in a given volume of a lattice. As a

result, [1-c] denotes the fraction of empty equivalent sites in a given volume, with N denoting the total number of occupied and unoccupied equivalent sites in a particular lattice volume.

By substituting (1.8) in (1.7) and realising that *n*, the number of mobile ions present within a given volume of lattice, is the product of *N* and *c*, the general formula (equation (1.9) is obtained describing ionic conductivity in a solid as a function of temperature[15].

$$\sigma T=[z/6][q^2/k]c[1-c]N\lambda^2\gamma\upsilon\exp[\Delta S_m/k]\exp[-\Delta H_m/(kT)] \quad (1.9)$$

ΔS_m (eV K^{-1}) and ΔH_m (eV) are ionic motion's entropy and enthalpy terms. It is possible to represent the fraction of the unoccupied sites, [*1-c*], with $[V_o]_s$ (expressed as a site fraction in the notation developed by Vink and Kröger). Vacancy concentration is usually expressed as a molar fraction. The molar fraction is equivalent to the site fraction in the case of MO type dopants only. Equation (1.9) can be expressed in the form of the Arrhenius relationship:

$$\sigma T = A\exp[-\Delta H_m/(kT)] \quad (1.10)$$

$$A=[z/6][q^2/k]([V_o^{\cdot\cdot}]_s)(1-[V_o^{\cdot\cdot}]_s)N\lambda^2\gamma\upsilon\exp[\Delta S_m/k] \quad (1.11)$$

Plotting log (σT) vs $1000/T$ theoretically give a straight line with slope= $-\Delta H_m/(kT)$ assuming that the $([V_o^{\cdot\cdot}]_s)(1-[V_o^{\cdot\cdot}]_s)$ term is temperature independent. The term enthalpy is frequently substituted by E_a, which stands for "general activation energy."

$$\sigma.T = A\exp(-E_a/kT) \quad (1.12)$$

Kilner[16] proposed that terms like z, N, and are unlikely to change considerably from one oxide to the next and that because q and k are constants, $[V_o]_s$ and ΔH_m are the most influential parameters controlling ionic conductivity. As a result of dopant-vacancy association, the $([V_o]_s)(1-[V_o]_s)$ term has been found to be temperature dependent[18]. Kilner and Steele postulated that electrostatic interactions between dopant cations and oxygen-ion vacancies affected the bound vacancies by making them unsuitable for contribution in the conduction

process, leading to a significant reduction in the number of free vacancies available in the crystal lattice[15][19][20]. As a result, at low temperatures, the free vacancies concentration is determined by the thermodynamic equilibrium between bound and free vacancies[16][20][21]. Kilner incorporated dopant-vacancy association enthalpy (ΔH_a) and entropy (ΔS_a) factors to the Arrhenius relationship to account for the occurrence of dopant-vacancy couplings. The activation energy value calculated from Arrhenius data has been demonstrated to be dependent on the migration (ΔH_m) and association ((ΔH_a) enthalpy components where considerable dopant-vacancy association occurs[15][22]. It is assumed that in dilute systems ($[V_o^{\cdot\cdot}] < 1\%$), vacancies have only one dopant cation in the neighbouring position, and as a result, only simple dopant-vacancy interactions are expected to occur at low temperatures[23][20]. The charge of the dopant influences the type of dopant-vacancy interaction. Using mass action and charge neutrality rules to the defect association equations below (1.13) and (1.14), and assuming that vacancies are fully associated at low temperatures, Kilner and Steele[20] demonstrated a thermodynamic relationship between free defects and dopant-vacancy associates. For systems where the host cation has an oxidation state of 4+ (Zr^{4+}, Ce^{4+}, Th^{4+}), it has been shown that the addition of dopants with a 2+ valency (Mg^{2+}, Ca^{2+}, Sr^{2+}) results in the creation of neutral dopant-vacancy associates (eq. 1.13), while for systems where dopants with a valency of 3+ are employed (Y^{3+}, Nd^{3+}, Gd^{3+}, Ho^{3+}, Yb^{3+}, Sc^{3+}…etc) charged dopant-vacancy associates form (eq. 1.14). Equations (1.13) and (1.14) are expressed in the Kröger-Vink notation.

$$Ca''_{Ce} + V_o^{\bullet\bullet} \leftrightarrow [Ca''_{Ce} + V_o^{\bullet\bullet}]^{\times} \quad (1.13)$$

$$Y'_{Ce} + V_o^{\bullet\bullet} \leftrightarrow [Y'_{Ce} + V_o^{\bullet\bullet}]^{\bullet} \quad (1.14)$$

In theory, the electrical conductivity of the neutral dopant-vacancy associations generated at low temperatures varies as a function of the square root of the dopant

concentration [20]. In addition, the activation energy term, E_a, is equal to the total sum of the migration enthalpy (ΔH_m) and one-half of the association enthalpy ($\Delta H_a/2$). The electrical conductivity of the charged associate is theoretically independent of dopant concentration, and the overall activation energy is the sum of the association and migration enthalpy factors[24]. During the development of thermodynamic expressions for the equilibrium between free defects and dopant-vacancy associates by Kilner and Steele [20], an approximation was made in which it was assumed that the concentration of dopant-vacancy associates was much greater than the concentration of free vacancies at low temperature. Kilner and Waters investigated the feasibility of the association between free defects and dopant-vacancy formation by re-examining the thermodynamic relationship[18].

1.7.2 Microstuructural Control

The total ionic conductivity of an electrolyte composition is influenced not only by the Arrhenius equation's parameters but also by its microstructure. Microstructural parameters such as pore size, pore concentration, pore location, grain size, phase assemblage, its distribution, and the concentration and location of impurities can all significantly impact the total ionic conductivity. The influence of each of the microstructural parameters depends on the powder processing, fabrication and sintering conditions employed to produce the ceramic. Besides the initial ceramic fabrication conditions, post-sintering annealing can often bring about significant changes in the microstructure and, therefore, the ionic conductivity of a ceramic. Microstructure has two functions in general: bulk and grain-boundary impacts. AC impedance spectroscopy (will be discussed in detail in chapter 2)[25]-[28] has been used to monitor changes in the microstructure by using the frequency domain to separate the grain

volume, and grain boundary impedances form the total impedance. Studies employing AC impedance techniques performed in the past have contributed largely to what is currently known about the influence of microstructure upon ionic motion through electrolyte materials.

Controlling phase assembly is also necessary to extract the highest ionic conductivity from an electrolyte composition and ensure that conductivity degradation is minimised over time at SOFC operating temperatures. Ionic conductivity performance in ceramic oxide materials is frequently affected by inhomogeneous phase distribution and the production of poorly conducting secondary phases. These effects can often be minimised with careful selection of dopant concentration, proper powder processing, fabrication, and sintering conditions. As previously stated, an electrolyte's long-term phase stability is required for stable SOFC power output. Significant formation of a poorly conducting phase over a period of time can harshly reduce the ionic conductivity of an electrolyte. Vlasov and Perfiliev[26] demonstrated that there are three sources of electrical conductivity degradation in an electrolyte composition based on their work in the ZrO_2-$YO_{1.5}$ system. These include (i) the formation of ordered phases, (ii) solute redistribution because of annealing in a two-phase field and subsequent production of a poorly-conducting material and (iii) altering contact resistivity present between grains in polycrystalline materials as a result of impurities present at the grain-boundaries. The first two causes of electrical conductivity degradation are related to phase stability and must be avoided by keeping electrolyte compositions in thermodynamically stable regions of the phase diagram. The existence of non-conducting impurity phases at grain boundaries[26][29] is the third source of electrical conductivity degradation.

The size and extent of pores inside the grain volume influence ionic conductivity as the pores act as resistive barriers to ionic mobility. The size and number of the pores should be as

small as feasible in an electrolyte composition since porosity levels > 5% will result in open or connected pores that will allow gas diffusion through the material [30][31]. Powder processing techniques have previously been investigated and optimised to generate homogenous oxide powders that yield sintered ceramic materials with densities more than 95% of their theoretical values. In the case of the ceramic electrolyte materials, powder processing must be carefully controlled to ensure that dopant oxides are homogeneously dispersed throughout the powders and also to produce powders of high sinterability [30]. Impurities should be kept to a minimum during any powder fabrication process. A number of different powder fabrication processes have been investigated in the past and include techniques such as milling of oxide powders, coprecipitation, sol-gel, and flame pyrolysis, combustions methods[32][33].

Traditionally, milling (wet or dry) of oxides have been employed in the preparation of ceramic powders; however, problems with homogeneity have been realised [33][29]. Furthermore, the quality of the raw oxides has a significant impact on the sinterability of the processed powder and the quantity of impurities present in sintered ceramics. The size of the particles precipitated and their size distribution are influenced by the preparation routes, temperature, and rate of cation solution injection[34][29]. To maximise the sinterability of a powder, it is typical for the precipitated particle size to be as small as possible (<< 1μm) and have a particle size distribution that will produce efficient packing in the green compact. After the drying of homogeneous precipitate, a calcination step is employed to convert the hydroxides to oxides[35].

However, the formation of agglomerates during the drying and calcination of the precipitate can reduce the sinterability of the powder, especially if the precipitate particle size

is very small (<< 1μm) [29]. As a result, agglomeration control techniques are frequently used in the fabrication process. To prevent hard agglomeration formation, a variety of drying procedures have been investigated, including solvent washing, sedimentation, freeze-drying, and hydrothermal treatment[29][31]. The green density in a compact is influenced by particle size, shape, size distribution, and compaction pressure.

Selection of suitable powder fabrication technique, control of processing parameters, and effective de-agglomeration, calcination can provide oxide powders that are both homogeneous and conducive to producing highly dense, sintered ceramics. Variations in phase assemblage within an electrolyte material normally solely affect grain volume impedance; however, the presence of grain-boundary phases can occasionally modify cation concentrations near the grain boundaries and, as a result, indirectly influence grain volume impedance. In a fully- or partially-stabilised, zirconia-based electrolyte composition, variation in the cation concentration in the grains close to the grain boundaries can result in significant changes in the phase assemblage in these areas. This may affect the ionic conductivity and result in unwanted and mechanically catastrophic phase changes. Thus, the impurity secondary phase segregated along the grain boundaries also diminishes the grain boundary conductivity of the systems[36].

So, powder processing, green ceramic fabrications, and sintering conditions must all be optimised in order to produce ceramic electrolyte compositions with high densities and increased ionic conductivity.

1.8 Present scenario of electrolyte materials for solid oxide fuel cell

Factors that influence the ionic conductivity of electrolytes have been identified as dopant type, size, and concentration. Furthermore, it is widely acknowledged that optimizing the

microstructure is critical for increasing ionic conductivity in electrolyte material. Many alternative electrolyte systems such as zirconia, ceria, lanthanum gallate, lanthanum aluminate, sodium bismuth titanate as well as bismuth oxide based systems have been examined as potential oxygen-ion conductors for SOFC applications to meet the aforementioned parameters. A comparative report of published articles based on electrolyte material from the last ten years is shown in Fig. 1.10(a). The number of publications on electrolyte materials keeps increasing, indicating that the work on solid electrolytes is highly demanded. Among all of these electrolytes, no. of publication for ceria and zirconia-based electrolyte are very high. The work reported on $Na_{0.5}Bi_{0.5}TiO_3$ is very less. $Na_{0.5}Bi_{0.5}TiO_3$ shows good conductivity, is not much expensive and operates at low temperatures. These properties made NBT a cost-effective substitute to other electrolytes. We have also explored another possible class of electrolyte material, tri-yttrium gallate. A comparative report of publication of a few prominent electrolyte materials is shown in Fig. 1.10(b).

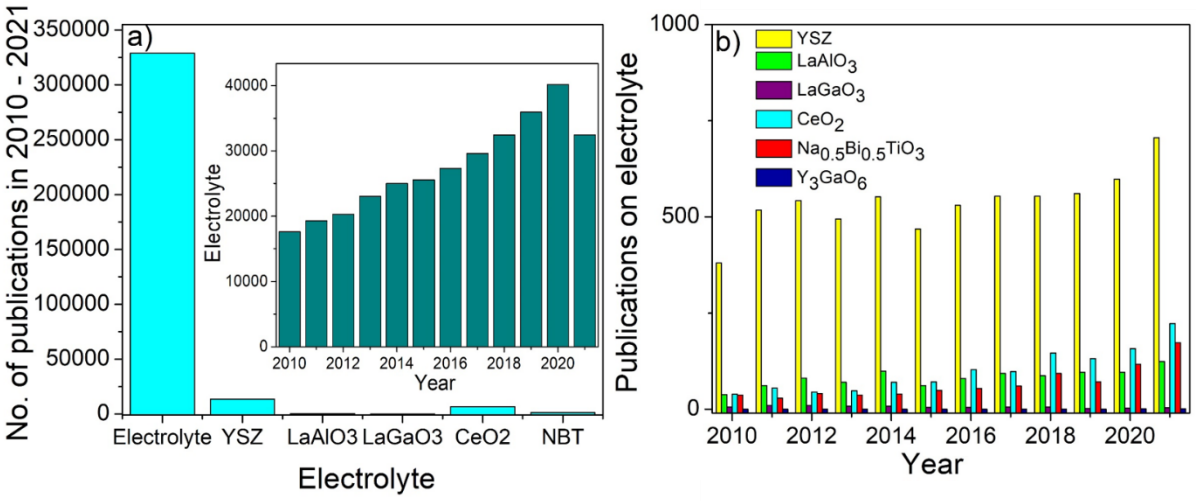

Figure 1.10. Present scenario of electrolyte materials

1.9 Materials for electrolytes

To achieve high ionic conductivity in electrolyte materials, materials must have an abundance of crystal defects, which result in low migration enthalpy and point defect disorder. These compounds contain metal cations that have a certain level of vibration because their sizes are much smaller than oxide ions, and the metal cations also possess a high valence charge, which prevents free movement within the network. Due to this phenomenon, local defects allow the ions to pass through the structure. The oxide ion conductors are classified into the following categories depending on the structural groups:

1.9.1 Fluorite structured electrolyte

The fluorite structured oxides are the traditional oxide ion-conducting electrolyte materials with the general formulae AO_2, where A is tetravalent cations. ZrO_2, CeO_2, ThO_2, HfO_2 and UO_2 are the few examples of oxides that crystallizes in the fluorite structure. Among these, only ZrO_2 and CeO_2 have been found to be interesting to the researchers as electrolyte materials. Fluorite electrolytes contain face-centred cubic arrangements of cations, and anions have tetrahedral sites. Figure 1.11 depicts the cubic fluorite structure of ZrO_2.

To achieve appreciable conductivity, oxygen vacancies are introduced in the system via substituting the host M^{4+} by lower valency acceptor cations. This can be given by the defect equation using Kroger Vink notation as:

$$D_2O_3 \xrightarrow{2MO_2} 2D'_M + 3O_O^X + 2V_{\ddot{o}} \qquad (1.15)$$

Diffusion of oxygen occurs when the oxide ions hop from their tetrahedral site to the adjacent oxygen vacancies. This type of migration is known as discrete hopping.

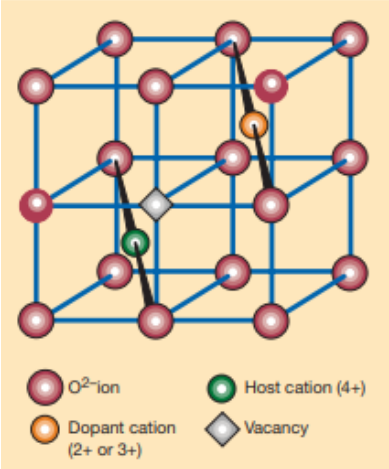

Figure 1.11: Fluorite structure[37]

1.9.1.1 Stabilized Zirconia

At present, the most widely investigated electrolyte is stabilized ZrO_2. Pure ZrO_2 exhibits very low conductivity due to the absence of adequate interstitial oxide ions and vacancies. Pure ZrO_2 exists in three polymorphs, i.e. monoclinic (RT to 1170 ºC), tetragonal (1170-2230 ºC), and cubic fluorite (>2370 ºC) [38]. All these transformations reverse down during cooling, followed by a large change in the volume. As a result, crack arises in the system upon cooling. The high temperature fluorite structure can be stabilized at room temperature by substituting large cation of lower valency at Zr site. Most common dopants are MgO, CaO, Y_2O_3, Sc_2O_3 and a few rare earth oxides. The dopants must have high solubility in zirconia and should be able to form a stable fluorite structure. Yttria stabilized zirconia is the most commonly used and possesses ionic conductivity of 0.1 S/cm at 1000 ºC. Yttria is added to stabilize the fluorite phase and increase the concentration of oxygen vacancies. Currently, most SOFC systems use stabilized zirconia (ZrO_2), especially yttria-stabilized zirconia (YSZ). This material offers an adequate level of oxide ion conductivity and is stable under both oxidizing and reducing conditions[39]. A number of literatures on YSZ shows that conductivity first

increases with the dopant concentration and then decreases for higher dopant concentration[27][40]. The decrease at higher dopant contents is due to the association of point defects, vacancy clustering, or electrostatic interaction, which reduces defect mobility and thus conductivity. Conventional zirconia-based electrolytes require an operating temperature of 800-1000 ºC. The operating temperature of an electrolyte depends on its ionic conductivity and the thickness of its layer. As a result, there are two methods for lowering the working temperature. The first is to minimise the YSZ electrolyte layer thickness, while the second is to look for alternate electrolyte materials with greater oxygen ion conductivities.

Several attempts have been made to identify new solid–electrolyte compositions in ternary systems[41]. Calcium, for example, can reduce the activation energy for migration when added to YSZ. It is also possible to improve the mechanical properties of zirconia solid electrolytes by adding small amounts of highly dispersed alumina. However, this leads to both increase and decrease in the conductivity of YSZ, depending on the doping concentration[42].

1.9.1.2 Doped Ceria

Ceria based electrolytes are crucial due to their better ionic conductivity than the zirconia-based electrolytes at relatively lower temperatures. They have fluorite structure and *Fm3m* space group over the entire temperature range from room temperature to the melting point of ceria. Undoped CeO_2 have negligible oxygen vacancies in their crystal structure, so the conductivity is low. In order to improve its conductivity, divalent or trivalent cations such as Ca^{2+}, La^{3+}, Sm^{3+}, Gd^{3+} etc., substitution has been investigated[43]. Studies revealed that the closer the ionic radii of dopant and host cations, the higher is the conductivity[44]. Among CeO_2 based materials, Gd and Sm doped ceria exhibit the highest conductivity. Doped ceria

electrolytes have much higher conductivity than that of stabilized zirconia at intermediate temperature.

However, despite its favourable ion transport capabilities, ceria had not been considered a viable fuel cell option until recently due to its high electronic conductivity[45]. The major limitations with this material is n-type electronic conductivity in the fuel environment and mechanical disintegration under high chemical potential gradient. These effects are less prominent at low temperatures, and hence these electrolytes are best suited for low and intermediate temperature applications.

1.9.2 Brownmillerite – type ceramics

The Brownmillerite structure having general formulae $A_2B_2O_5$, where A and B are cation sites, shows fast oxide ion conduction at temperature above 930 ºC[46]. It is derived by detaching 1/6th of the oxygen vacancies in a perovskite structure and then ordering the oxygen vacancies. The structure consists of an alternate perovskite layer of corner-sharing BO_6 octahedra and layer of BO_4 tetrahedra (Fig. 1.12)[47]. The vacancy forms a 1D diffusion path, allowing ion migration along with tetrahedral layers. With the temperature increase, brownmillerites undergo phase transition from the orthorhombic phase to the tetragonal phase at ~ 925 ºC and to distorted cubic at ~ 1040 ºC[48]. The distorted cubic phase results in fast oxide ion conduction because of the enormous number of vacancies in the system.

The brownmillerites manifests different type of conductivity under different atmosphere, viz. in moderate P_{O_2} and dry atmosphere, it shows oxide ion conductivity (ionic conductivity). They exhibit mixed ionic and p-type electrical behaviour under oxidizing conditions, while protonic conduction is observed in the H_2O gas mixture. Brownmillerites are sensitive to

humidity. When subjected to humidity below 300 ºC, Schober et al. observed the structural transformation of $Ba_2In_2O_5$ to $Ba_2In_2O_5.1H_2O$[49].

$Ba_2In_2O_5$ shows mixed conductivity with dominating oxide ion conductivity in dry air. The increase in the temperature causes a structural transition to the distorted perovskite phase at 930 ºC, increasing ionic conductivity. Doping with a higher valency cation, such as Ce^{4+}, Zr^{4+}, Hf^{4+}, Sn^{4+}, can stabilize the deformed perovskite phase, resulting in an increase in ionic conductivity[50][51]. Kakinuma et al. have reported the ionic conductivity of La^{3+} and Sr^{2+} substituted $Ba_2In_2O_5$. The conductivity of this system was comparable to YSZ at 800 ºC.

Besides oxygen vacancy concentration, ionic conductivity is also influenced by the unit cell free volume given by

$$\text{Unit cell-free volume} = abc - \Sigma m_i \frac{4}{3} \Pi r_i^3 \qquad (1.16)$$

where a,b,c are the unit cell parameters, r_i is ionic radii, and m_i is the chemical composition of ions. In $(Ba_{1-x-y}Sr_xLa_y)_2In_2O_{5+y}$, the unit cell volume and conductivity are found to increase linearly with the Sr^{2+} content. Some more compositions have been investigated in this category of electrolytes[52].

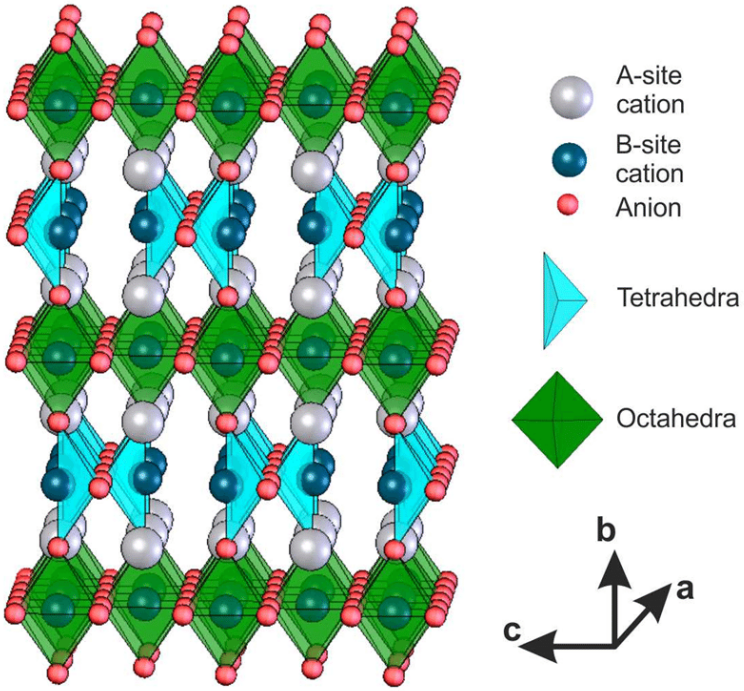

Figure 1.12: Brownmillerite crystal structure[53]

1.9.3 $La_2Mo_2O_9$(LAMOX) based electrolyte materials

$La_2Mo_2O_9$ (LAMOX) based materials was first reported as fast oxide ion conductor by Lacorre et al. in 2000[54]. The oxide ion conductivity of LAMOX was comparable to the stabilized zirconia at 800 ºC. It exhibits a phase transition from a nonconductive monoclinic α form to the highly conductive cubic β form at a temperature around ~ 580 °C, similar to Bi_2O_3 based oxides. Because of the phase transition and the possible reducibility of molybdenum in a fuel environment, researchers have investigated a number of substitutions for both molybdenum and lanthanum sites. Substitution on both the sites suppresses the transition and improves the stability in reducing atmosphere[55][56].

The ionic transport in these materials occurs via loan pair substitution mechanism [57]. The structure of β-$SnWO_4$ is a suitable model for understanding the oxygen transport

mechanism in $La_2Mo_2O_9$[58]. As depicted in Figure 1.13 in β-$SnWO_4$, loan pair of Sn^{2+} cation distorts the octahedral environment and occupies a volume similar to O^{2-} ion. In $La_2Mo_2O_9$, La^{3+} cation has size similar to Sn^{2+} cation but without loan pair. When La^{3+} is placed at Sn^{2+} site, two extra vacancies appear, and extra oxygen atom occupies one of the vacancies to compensate the cationic valency, and the Mo atom replaces W. This extra vacancy becomes available for the oxide ion conduction.

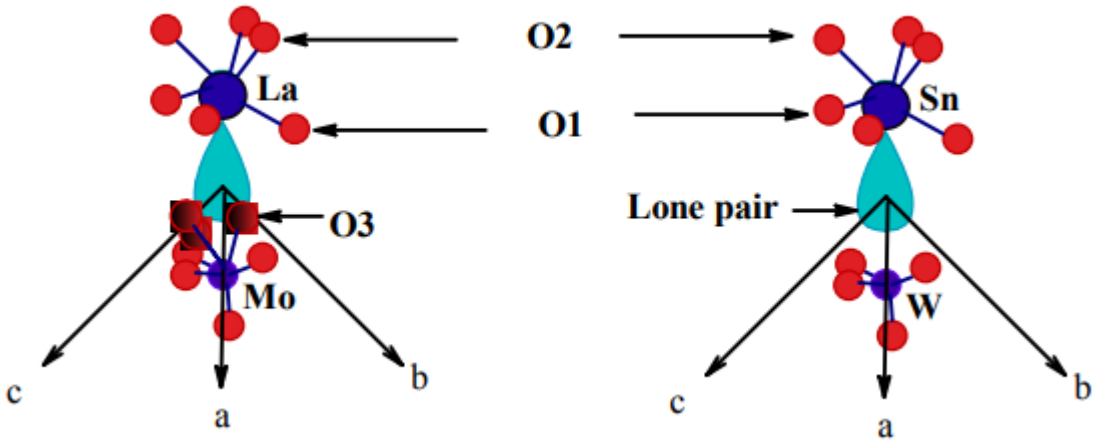

Figure 1.13: Comparison of the cationic environment of β-$SnWO_4$ and β-$La_2Mo_2O_9$[59]

Subasri et al. have explored both the ionic and electronic conductivity of $La_2Mo_2O_9$ as as a function of temperature and observed the conductivity to be ~ 3 order of magnitude lower than that reported by Loccore et al.[60], [61]. However, Subasri et al. further suggested that the high conductivity observed by Laccore et al. was probably because of the impurity phase present in the $La_2Mo_2O_9$ sample. The main disadvantage with $La_2Mo_2O_9$ based material is mixed type of conductivity at lower partial pressure and at elevated temperatures.

1.9.4 Apatite structure

Interest in the rare-earth-based apatite structure has gained significant attention because of its high oxide ion conductivity and chemical stability. A vital prerequisite for fast ionic conduction is high symmetry in the lattice.

The general formula for apatite-based materials is $A_{10-x}(MO_4)_6O_2$, where A is a rare earth or alkaline earth cations, and M is p-block element. The family of apatite based conductors mainly consists of $Ln_{9.33+x}(Si/GeO_4)_6O_{2+3x/2}$. The structure consists of isolated MO_4 tetrahedra arranged to form *x* anion and La channels running parallel to the c axis (Fig. 1.14) [62]. The oxide ion channels present at the central position also participate in the ionic conductivity. The rare earth cations are placed at 7 and 9-coordinate cavity sites, and additional oxide ions run through the structure, which is accountable for the high oxide ion conductivity. Theoretical atomistic modelling suggests that the conduction in $La_{9.33}(SiO_4)_6O_2$ and $La_8Sr_2(SiO_4)_6O_2$ occurs via intersticial and vacancy mechanism[63]. For interstitial oxygen migration, the speculated pathways appear to be a non-linear "sinusoidal type" process, whereas the vacancy mechanism is expected to follow a direct linear path. According to the modelling results, the peripheries of the oxide ion channel neighbouring to the SiO_4 units are the most energetically favourable interstitial site[64]. The electrical conductivity of many apatite-based systems is reported in the literature[65]. Among reported rare earth apatite, lanthanum silicates exhibit higher ionic conductivity than germinate based apatite, and the conductivity obtained is ionic in the wide range of oxygen partial pressure[66][67]. The triclinic crystal structure of silicate apatite transforms to a hexagonal cell at high temperatures, lowering the activation energy.

Moreover, oxygen excess apatite also shows higher conductivity, indicating interstitial oxide ions help to enhance the conductivity of oxide ions. A large number of compositions have been examined; however, most of the work is focused on the doped lanthanum silicate, i.e., $La_{9.33+x}(SiO_4)_6O_{2+3x/2}$[65][68].

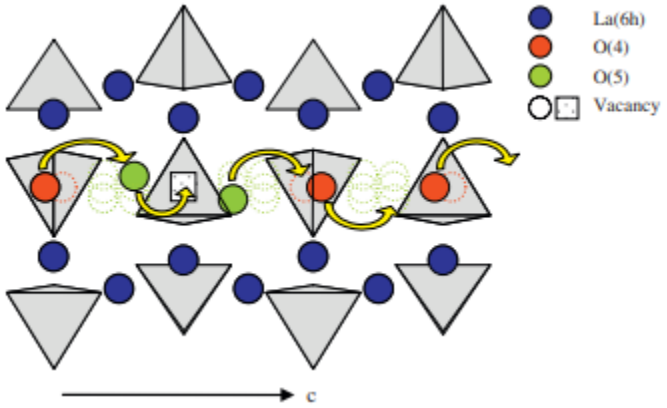

Figure 1.14: Structural defects position and conduction mechanism[69]

1.9.5 Perovskite-based ceramics

Perovskite type oxides (with the general chemical formulae, ABO_3) were investigated as the oxide ion conductors by various groups of researcher[70]. As illustrated in Fig. 1.15(a), an ideal perovskite have a cubic structure with 12 coordinated large cations of A and 6 coordinated small cation of B. A variety of combinations of 1+5 can achieve the total charge on A and B (+6), 2+4, 3+3, and also in many more complex ways, such as $A(B'_{1/2}B''_{1/2})O_3$, $(A'_{1/2}A''_{1/2})BO_3$. The cubic structure shows the BO_6 octahedra form a corner-shared network, with the voids filled by cation A. The cubic structure often distorts to rhombohedral, orthorhombic, monoclinic, or tetragonal symmetry due to the tilting and stretching of the BO_6 octahedra.

Previously, it was thought that oxide ion conduction occurs via a standard hopping mechanism that involves the rapid movement of vacancies. This statement, however, was not backed up by any experimental evidence. In 1995, Cherry et al. used the defect energy estimate to create an aping energy profile[71]. In this, a saddle point configuration was developed, from which the energy barrier for oxygen ion migration was calculated. In this model, migrating ion is predicted to migrate through the triangle created by two A-site cations and one B-site cation in this model. The repulsive interaction was found to reduce apparently by the relaxation or outer movement of the cations.

Furthermore, since the available space in the perovskite lattice and the location of ions on the lattice prevent interstitial diffusion due to the high energy barrier > 1.5 eV, it was suggested that no interstitial diffusion could occur. So the ionic diffusion in the perovskite-type lattices such as $LaGaO_3$, $LaAlO_3$, $Na_{0.5}Bi_{0.5}TiO_3$, etc., must occur via migration of oxide ions jumping into the adjacent vacant site along the edges of BO_6 octahedra, with minimum migration barrier (Fig. 1.15 (a)). Neutron diffraction studies and theoretical atomistic calculations have additionally affirmed that the oxide ion migration doesn't take a straight route, and the saddle point of the curved path stay away from the neighbouring cations[72]–[74].

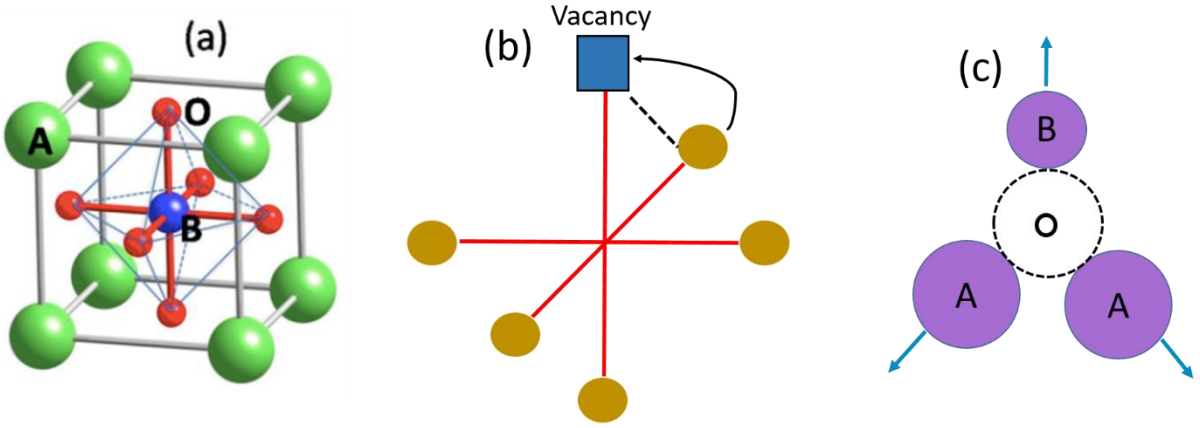

Figure 1.15: (a) Perovskite structure ABO_3 **(b)** Schematic of the curved pathway of oxide ion migration along the BO_6 octahedron (c) Saddle point configuration of oxide ion migration showing relaxation

The ionic radii of the A and B cation is an essential factor for the perovskite materials, as they significantly influence the ionic conductivity. Theoretical calculations reveal that the lower migration barrier can be achieved by increasing the size of the B cation (E_{max} at ~ 0.75Å) and decreasing the size of the A cation (E_{max} at ~ 0.95Å). The geometrical limits given by Goldschmidt for the A and B site cation in terms of the tolerance factor as:

$$t = \frac{(r_A + r_0)}{\sqrt{2}(r_B + r_0)} \qquad (1.17)$$

where r_A, r_O, and r_B are the ionic radii of the cation A, oxygen and cation B, respectively. For 0.75 < t <1.0, the perovskite structure is stable. Cherry et al. has established a correlation between the tolerance factor and the calculated migration energies and found that migration energy is minimum at t = 0.81[71]. The minima in the value of tolerance factor show equilibrium between the relaxation of A and B cation at the saddle point configuration, which is an important parameter for achieving minimum energies for oxide ion migration. Perovskite oxides possess minimum migration enthalpy for t = 0.81, and the migration energy increases with the value of t above 0.81.

Incorporation of acceptor dopants at A site of ABO_3 type perovskite oxides such as Mg^{2+}, Ca^{2+}, Sr^{2+}, Ba^{2+}has been reported to enhance the ionic conductivity and catalytic activity [37][75]–[80]. The depression in the effective valency at A-site generates oxygen vacancies as compensating defects, increasing the ionic conductivity. Among all the divalent dopants except $LaCoO_3$, doping with the Sr^{2+} results in maximum conductivity as the tendency for cluster formation is low [71]. The oxygen vacancies get trapped by the dopant and the host cation due to the elastic and electrostatic interaction between them, resulting in the reduction of mobile vacancies concentration [81].

1.9.6 Sodium Bismuth Titanate ($Na_{0.5}Bi_{0.5}TiO_3$)

Sodium bismuth titanate (NBT), ferroelectric material [82], has attracted the SOFC electrolyte research community since 2014 [70][83]. It was first reported in 1960 and has received considerable attention in recent years[84]. Extensive research has been done on this material, but the research community still debates on the structure of NBT at room temperature, whether it has monoclinic structure (*Cc*) rhombohedral (*R3c*) [85]-[89]. Nevertheless, in IT-SOFC's operating range, 550-700 °C, the NBT transforms into a non-ferroelectric-cubic structure, which is ideal for electrolyte applications[89]. NBT is a good ionic conductor with transference number t_{ion}> 0.9. Li et al. reported that conductivity in NBT is primarily because of the oxygen vacancies[70]. Stoichiometric NBT show low conductivity, but with the slight non-stoichiometry and doping, the conductivity drastically improves. Sung et al. and Hiruma et al. have reported that the electrical conductivity of NBT is highly sensitive to the nominal variation in A-site cation stoichiometry and can result in more than three orders of magnitude change in conductivity[90]. Processing related variation also profoundly contribute to the total oxygen vacancy concentration. There is a consensus that oxygen vacancy mobility plays a very

important role in NBT, and this is due to the vacancies that are created from the loss of Bi_2O_3 during processing, the increased oxygen mobility of the weak Bi-O bond, and the high polarizability of Bi^{3+} ions. Higher oxide ion conductivity has been achieved in Bi-deficient NBT in contrast to the Bi-excess NBT. Based on various defect mechanisms, NBT can exhibit three different types of electrical behaviour, i.e., oxide ion conduction (type Ⅰ), mixed type conduction (type Ⅱ), and insulating/dielectric type conduction (type Ⅲ). Like ionic conduction in the perovskite-based oxides, conduction in NBT is mediated through the vacancy diffusion mechanism where the vacancy migrates between two adjacent sites along the edges of TiO_6 octahedra known as "saddle point" [91]. He et al. have computationally predicted the oxygen vacancy migration barrier along different paths in NBT[92]. To enhance the ionic conductivity of NBT, several doping strategies has been reported. Li et al. investigated the 2% Mg-doped bismuth deficient $Na_{0.5}Bi_{0.49}TiO_{3-\delta}$ and showed two order enhancement in the conductivity as compared with NBT[70]. Yang et al. examined the influence of A-site divalent doping of cations such as Ca^{2+}, Ba^{2+}, and Sr^{2+} on the electrical conductivity of $Na_{0.5}Bi_{0.49}TiO_{3-\delta}$[93]. Among them, Sr^{2+} has been identified as the most effective dopant for enhancing grain conductivity because of its good polarizability, smaller size mismatch with the host, and weak metal-oxygen bond strength. The grain conductivity of $Na_{0.5}Bi_{0.47}Sr_{0.02}TiO_{3-\delta}$ was found to be 5.13 $mS.cm^{-1}$ at 500 °C, which is 26% more than $Na_{0.5}Bi_{0.49}Ti_{0.98}Mg_{0.02}O_{3-\delta}$[93]

1.9.7 Pyrochlores based ceramics

Pyrochlores are the class of ion-conducting materials having general formulae $A_2B_2O_7$. They are derived from the oxygen-deficient fluorite, also known as defect fluorite superstructure. Pyrochlores' crystal structure is the fluorite superstructure (MX_2), with ordered A and B cations and one-eighth of the anions absent[94][95]. The vacant sites provide the

pathway for the migration of oxide ions. Kharton et al. in 2009 reported that pyrochlore to fluorite transition is favoured on reducing the size of cation at A site[96]. The structure of the ordered pyrochlore lattice is transformed into the disordered anion deficient fluorite M_4O_7 (M represents A or B)[68] as the cation size decreases[97]. Thermally-induced or irradiated order-disorder transitions are also possible [97][98]. For the ionic radii ratio of A and B cation ~ 1.46, $Gd_2Zr_2O_7$ lies at the edges of the ordered pyrochlore and defective fluorite system.

The ionic conductivity of the pyrochlore system is comparable to that of YSZ (e.g. $Gd_2Zr_2O_7$ ~ $5x10^{-2}$ S/cm). The conductivity of pyrochlores can be tuned by thermal treatment or chemical substitution[99][100]. Among various investigated pyrochlores, $Gd_{2-x}Ca_xTi_2O_{7-\delta}$ exhibit the highest conductivity. The pyrochlore materials are mostly used as protective films on lanthanum gallate and ceria based electrolytes. Moreover, with the tolerable value of CTE, they possess good compatibility with the other cell components[10].

1.9.8 δ-Bi_2O_3 based ceramics

δ-Bi_2O_3based ceramic exhibits fcc structure and is perhaps the best oxide ion conductor in the fluorite structured electrolyte category[101]. Bi_2O_3 exists in two stable polymorphs form, i.e. monoclinic α and cubic δ phase. The α→δ transition occurs at a temperature of around 720 ℃, resulting in a three-fold increase in ionic conductivity. The δ phase is stable in the temperature range of 730 ºC to 804 ºC. The problem with Bi_2O_3 is that it reduces to metallic Bi^0 when reducing gases such as CH_4 or H_2 are present. In order to stabilize its structure at lower temperature, aliovalent dopant cation such as La^{3+}, Y^{3+}, Er^{3+} etc., has been used [102] [103].

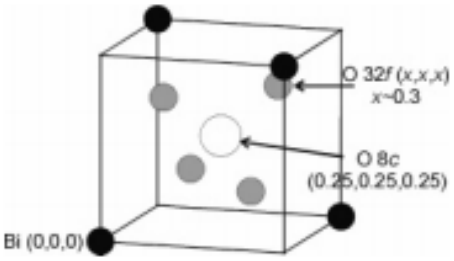

Figure 1.16: Visualization of δ-Bi_2O_3 unit cell[104]

The structure of δ-Bi_2O_3 consists of two partially occupied O-sites: 32*f* (*x, x, x*) and 8*c* (1/4, 1/4, 1/4) and with x ≈ 0.3 as shown in Fig. 1.16. The occupancy of the 32*f* site increases with the ageing, which leads to an increase in the local vacancy ordering. Verkerk et al. have reported that the high-temperature cubic phase can be stabilized at room temperature by contracting the structure with the help of smaller size cation doping[104]. Small amounts of dopant can compensate for large ionic radius mismatch between the dopant and Bi^{3+} cation. On the other hand, if the size mismatch is less, a large concentration of dopant is required. But, doping also lowers the conductivity, especially at low temperatures as compared to the parent compound. At the fixed level of doping, oxide ion conductivity increases with the increase in the size of Ln^{3+} because of the comparatively larger size of Bi^{3+}. The maximum stabilization limit for maintaining the fluorite structure increases with the size of the lanthanide cation, lowering the ionic conductivity[104].

The disadvantage of the Bi_2O_3 based materials are the tendency to reduce in Bi^0 under reducing atmosphere, corrosion, volatilization, and poor mechanical strength. Various bilayer approaches were employed to overcome these challenges, where Bi_2O_3 was kept on the cathode side and a stable electrolyte layer (like doped CeO_2) on the anode side[105], [106].

A study by Punn et. al. showed that the oxide ion conductivity of stabilized δ-phase in $Bi_{12.5}Ln_{1.5}ReO_{24.5}$ (Re stands for Rhenium) was improved using large size dopant cations At

300 ºC, $Bi_{12.5}La_{1.5}ReO_{24.5}$is reported to exhibit the highest conductivity in the doped Bi_2O_3 category[107]. Furthermore, the required activation energy for the oxide ion migration in samples containing large size lanthanides is less at lower temperatures than the stabilized phase[54].

Another family of $Bi_2O_3$is bismuth metal vanadium oxide $Bi_4V_2O_{11}$, known as BIMEVOX (Bi-Bismuth, Me- metal, V- Vanadium, Ox- Oxygen). It consists of alternate layers of $Bi_2O_2^{2+}$ and $VO_{3.5}^{2-}$ and belong to aurivillius series of family. Ionic conduction in these materials occurs because of oxygen vacancies present in the perovskite layers. $Bi_2V_{1-X}Me_XO_{5.5-\delta}$ (Me = Cu, Ni) based solutions have been reported to possess the highest ionic conductivity. However, in spite of high conductivity, they encounter similar redox problems as that of Bi_2O_3 and these issues can be resolved by developing the multilayer electrode structure[108].

1.10 Tri-Yttrium Gallate (Y_3GaO_6)

Recently, another class of oxide ion conductors, Y_3GaO_6 has been explored in search of new electrolytes. RE_3GaO_6 series were first investigated by Carruthers et al. and Schneider et al. for their magnetic and optical properties[109]-[111]. To explore this, we investigated the bond valence energy landscapes (BVEL) of O^{2-} ions diffusion in a few yttrium containing oxide materials[112]. The BV-based energy barrier for Y_3GaO_6 was ~ 0.54 eV along the c-axis of the crystal structure.Y_3GaO_6 is yttrium oxy-monogallate, and its chemical formulae can also be written as $Y_3O_2GaO_4$. As a result, Y_3GaO_6 was chosen for future study because it has a lower energy barrier than other Y-containing oxide systems. Y_3GaO_6 crystallizes in the orthorhombic structure with space group $Cmc2_1$. This structure (with lattice parameters a = 8.843 Å, b = 11.098 Å, and c = 5.398 Å) contains 12-Y (the four Y ions occupy *4a*, and eight

Y ions occupy *8b* Wyckoff sites, respectively), 24-O and 4-Ga atoms in a unit cell[113] which are made up with two types of edge-sharing YO_7 pentagonal bipyramids polyhedra making a three-dimensional framework and with a GaO_4 tetrahedron (shown in Fig. 1.17). It means the Y^{3+} cations get localized in two different asymmetric sites with sevenfold coordination, and the Ga^{3+} cation form distorted oxygen tetrahedral[113]. Ga^{3+} is bonded to four O^{2-} atoms to form GaO_4 tetrahedra that share a corner-corner with one YO_7 pentagonal bipyramid and an edge-edge with one YO_7 pentagonal bipyramid. According to a recent study, the Ln_3GaO_6 (Ln = La, Nd, Gd, Tb, Ho, Dy, Er, or Lu) system could be a suitable oxide ion conducting system[114]. However, researchers have previously conducted a few experimental experiments on various variants of these species. Purohit et al. [115] identified Nd_3GaO_6-based systems as a new class of oxide ion conductors. They used Ca^{2+} and Sr^{2+} as dopants at the Nd-site and discovered a three-fold increase in conductivity. A recent investigation on the synthesis and electrical characteristics of alkali-earth-substituted Gd_3GaO_6 shows a total oxide-ion conductivity, $\sigma_{800\,^{o}C} = 1\times10^{-2}$ Scm^{-1} for Ca^{2+} substitution [116].

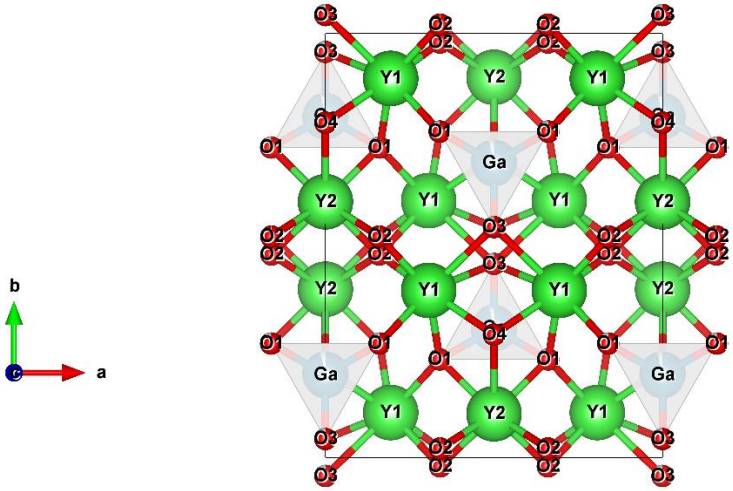

Figure 1.17: Crystal structure of Y_3GaO_6 along 001 direction showing GaO_4 tetrahedra. Green, red and blue sphere represents the Y^{3+}, O^{2-}, and Ga^{3+} ions, respectively. Y1 and Y2 of the crystallographic positions of Y

1.11 Objective of the Present Research Work

The main objective of the present research work is to investigate the physical properties (especially electrical properties) of a few cost-effective electrolyte materials for SOFCs applications in the intermediate temperature range. For this purpose, sodium bismuth titanate and tri-yttrium gallate have been selected as the electrolyte material. The structural, thermodynamical, optical, and electrical properties of these materials were studied, and a correlation among them is established. In order to meet the above objectives, it has been planned to:

1. Synthesize sodium bismuth titanate at various sintering temperatures and study the effect of temperature optimization on the structural, morphological, electrical properties using various characterization techniques and its conduction mechanism.
2. Study of ion dynamics and conduction mechanism of non-stoichiometric $Na_{0.5}Bi_{0.5}TiO_{3-\delta}$.
3. Develop Bi-deficient Mg^{2+}-doped sodium bismuth titanate sample using polyol mediated synthesis method and study the oxide ion migration behaviour with functional properties.
4. Synthesize and Investigate alkaline earth metal doped tri-yttrium gallate (Y_3GaO_6) as a new electrolyte material for solid oxide fuel cell using solid-state reaction route and study its physical properties.
5. Examine the consequences of calcium substitution on the structural and electrical properties of Y_3GaO_6.

Details of the synthesis and characterization techniques for the studied systems are given in the next chapter. The results of the present investigation are described in the subsequent thesis chapters.